Small-Scale Effect on the Static Deflection of a Clamped Graphene Sheet

G. Q. Xie[1], J. P. Wang[2], Q. L. Zhang[1]

Abstract: Small-scale effect on the static deflection of a clamped graphene sheet and influence of the helical angle of the clamped graphene sheet on its static deflection are investigated. Static equilibrium equations of the graphene sheet are formulated based on the concept of nonlocal elastic theory. Galerkin method is used to obtain the classical and the nonlocal static deflection from Static equilibrium equations , respectively. The numerical results show that the static deflection and small-scale effect of a clamped graphene sheet is affected by its small size and helical angle. Small-scale effect will decrease with increase of the length and width of the graphene sheet, and small-scale effect will disappear when the length and the width of graphene sheet are both larger than 200 um.

1   Introduction

Since carbon nanotube was discovered by Iijima (1991), it has shown a broad application prospect in various fields because of its high mechanical strength, strong energy storage and catalytic effect etc. Due to the surface effect and the small-scale effect of nanomaterials, classical continuum mechanics will lead to an inaccurate result when it is used to solve the mechanics problem of nanomaterials. Fortunately, the nonlocal theory given by Eringen (1972) can remove the shortcoming of classical continuum mechanics. Based on the nonlocal theory, Zhang, Liu, and Wang, (2004) studied the buckling of multi-walled carbon nanotube. Xie, Han, and Long (2006, 2006, 2007) investigated the small scale effect and the vibration of carbon nanotube. Wang (2011) used a modified nonlocal beam model to study vibration and stability of nanotubes conveying fluid. Hybrid nonlocal beam model [Zhang,

---

[1] Civil Engineering college, Hunan University of Science and Technology, Xiangtan 411201, China
[2] Mianyang Vocational and Technical College, Mianyang 621000, China
Corresponding author. E-mail: 1020095@hnust.edu.cn

Wang, and Challamel (2009)] was employed to study bending, buckling, and vibration of micro/nanobeams. Reddy (2010) presented nonlocal nonlinear formulations for bending of classical and shear deformation theories of beams and plates. Fang, Zhen, and Zhang (2013) carried out nonlinear vibration analysis of double-walled carbon nanotubes based on nonlocal elasticity theory. Liang and Han (2014) gave prediction of the nonlocal scaling parameter for graphene sheet. Recently, Miandoab, Yousefi-Koma, and Pishkenari (2015) used nonlocal and strain gradient based model to study the electrostatically actuated silicon nano-beams. Zhao and Shi (2011) used an improved molecular structural mechanics model to study poisson ratios of single-walled carbon nanotubes.

In this paper, a nonlocal model of nanoplate is developed for the static deflection of graphene sheet. Small-scale effect on the static deflection of a clamped graphene sheet is investigated.

2   Formulation

2.1   *Nonlocal stress tensor*

In Eringen nonlocal elasticity model, Eringen (1983) considered that the physics of material bodies whose behavior at a material point is influenced by the state of all points in the body. This result is in accordance with atomic theory of lattice dynamics and experimental observations on phonon dispersion. The most general form of the nonlocal constitutive equation involves an integral over the entire region of interest.

For homogeneous and isotropic elastic solids, the nonlocal constitutive equation is

$$\boldsymbol{\sigma}(\boldsymbol{x}) = \boldsymbol{C}_0 : \int_V \alpha\left(\left|\boldsymbol{x}' - \boldsymbol{x}\right|, \tau\right) \boldsymbol{\varepsilon}\left(\boldsymbol{x}'\right) dV\left(\boldsymbol{x}'\right) \tag{1}$$

Where symbols ':' is the double dot product, $\boldsymbol{C}_0$ is the elastic modulus matrix of classical isotropic material, $\boldsymbol{\sigma}(\boldsymbol{x})$ denotes the nonlocal stress tensor at $\boldsymbol{x}$, and $\boldsymbol{\varepsilon}(\boldsymbol{x}')$ is the strain tensor at any point $\boldsymbol{x}'$ in the body. The kernel function $\alpha\left(\left|\boldsymbol{x}' - \boldsymbol{x}\right|, \tau\right)$ is the nonlocal modulus, $\left|\boldsymbol{x}' - \boldsymbol{x}\right|$ is the Euclidean distance, and $\tau = e_0 a / l$, where e_0 is a constant appropriate to each material, a is an internal characteristic size (e.g. length of C-C bond, lattice spacing, granular distance etc.) and l is an external characteristic size (e.g. crack size, wave length etc.). The volume integral in Eq. (1) is over the region V occupied by the body. However, e_0 and l of graphene sheet have not been found in theoretical or experimental literature.

Based on nonlocal elasticity model, we chose a representative element of graphene sheet shown as Fig. 1.

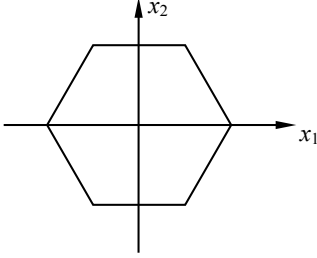The stress of a reference point $\boldsymbol{x}$ in the representative element can be expressed as
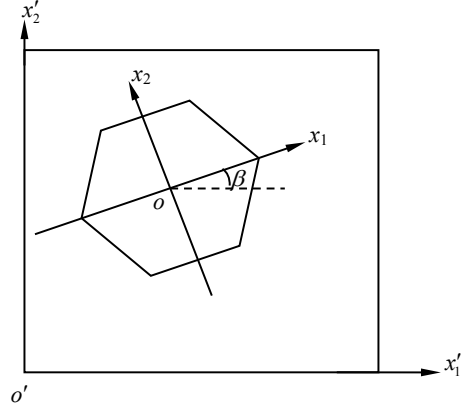
Figure 1: A representative element of graphene sheet.

Figure 2: A helical graphene sheet.

Taylor series

$$\sigma_{ij}(x_1,x_2) = \sigma_{ij}(0,0) + \frac{\partial \sigma_{ij}(x_1,x_2)}{\partial x_1}\Big|_{\substack{x_1=0 \\ x_2=0}} x_1 + \frac{\partial \sigma_{ij}(x_1,x_2)}{\partial x_2}\Big|_{\substack{x_1=0 \\ x_2=0}} x_2$$
$$+ \frac{1}{2!}\frac{\partial^2 \sigma_{ij}(x_1,x_2)}{\partial x_1^2}\Big|_{\substack{x_1=0 \\ x_2=0}} x_1^2 + \dots \tag{2}$$

To take the average of $\sigma_{ij}(x_1,x_2)$ over the representative element, in terms of the symmetry of the representative element, we have

$$\langle \sigma_{ij}(x_1,x_2)\rangle = \left(1 + 0.208l^2\nabla^2\right)\sigma_{ij}(0,0) \tag{3}$$

Where l is the length of C-C bond.

Inversion of eq. (3) yields

$$\sigma_{ij}(0,0) = \left(1 - 0.208l^2\nabla^2\right)\langle \sigma_{ij}(x_1,x_2)\rangle \tag{4}$$

Where $\langle \sigma_{ij}(x_1,x_2)\rangle$ is the nonlocal stress tensor.

2.2 Geometric equations

A helical graphene sheet shown as Fig. 2, (x_1, x_2) is the local coordinate system, and (x_1', x_2') is the global coordinate system. x_1' and x_2' are parallel to both sides of the graphene sheet,respectively.

Geometric equations of the helical graphene sheet in the global coordinate are

$$\varepsilon_{i'j'} = -zw_{,i'j'} \tag{5}$$

Where w is the static deflection of the graphene sheet, $w_{,i'j'} = \frac{\partial^2 w}{\partial x_i' \partial x_j'}$.

According to the transformation relationship of strains, we have

$$\varepsilon_{ij} = l_{ij'} \varepsilon_{i'j'} l_{i'j} \tag{6}$$

Where

$$\left. \begin{array}{l} l_{ij'} = \cos \angle \left(x_i, x_j' \right) \\ l_{i'j} = \cos \angle (x_i', x_j) \end{array} \right\} \tag{7}$$

$$\varepsilon_{ij} = -zw_{,ij} \tag{8}$$

2.3 Nonlocal constitutive equation

Based on Eq. (4), the nonlocal constitutive equations of graphene are rewritten as

$$
\begin{aligned}
\sigma_{11} - 0.208l^2 \frac{\partial^2 \sigma_{11}}{\partial x_1^2} &= \frac{E}{1-\mu^2} \left[\varepsilon_{11} + \mu \varepsilon_{22} \right] \\
\sigma_{22} - 0.208l^2 \frac{\partial^2 \sigma_{22}}{\partial x_2^2} &= \frac{E}{1-\mu^2} \left[\varepsilon_{22} + \mu \varepsilon_{11} \right] \\
\left(1 - 0.208l^2 \nabla^2 \right) \sigma_{12} &= \frac{E}{1+\mu} \varepsilon_{12}
\end{aligned}
\tag{9}
$$

Where E is the elastic modulus of graphene, and μ Poisson's ratio.

Eq. (9) can be approximately expressed as

$$
\begin{aligned}
\sigma_{11} &= \frac{E}{1-\mu^2} \left(1 + 0.208l^2 \frac{\partial^2}{\partial x_1^2} \right) \left[\varepsilon_{11} + \mu \varepsilon_{22} \right] \\
\sigma_{22} &= \frac{E}{1-\mu^2} \left(1 + 0.208l^2 \frac{\partial^2}{\partial x_2^2} \right) \left[\varepsilon_{22} + \mu \varepsilon_{11} \right] \\
\sigma_{12} &= \frac{E}{1+\mu} \left(1 + 0.208l^2 \nabla^2 \right) \varepsilon_{12}
\end{aligned}
\tag{10}
$$

Substituting Eq. (6) into Eq. (10), we have

$$
\begin{aligned}
\sigma_{11} = &-\frac{Ez}{1-\mu^2} \left[1 + 0.208l^2 \left(\cos^2 \beta \frac{\partial^2}{\partial x_1'^2} + 2 \sin \beta \cos \beta \frac{\partial^2}{\partial x_1' \partial x_2'} + \sin^2 \beta \frac{\partial^2}{\partial x_2'^2} \right) \right] \\
& \left(l_{1i'} \frac{\partial^2 w}{\partial x_i' \partial x_j'} l_{1j'} + \mu l_{2i'} \frac{\partial^2 w}{\partial x_i' \partial x_j'} l_{2j'} \right) \\
\sigma_{22} = &-\frac{Ez}{1-\mu^2} \left[1 + 0.208l^2 \left(\sin^2 \beta \frac{\partial^2}{\partial x_1'^2} - 2 \sin \beta \cos \beta \frac{\partial^2}{\partial x_1' \partial x_2'} + \cos^2 \beta \frac{\partial^2}{\partial x_2'^2} \right) \right]
\end{aligned}
$$

$$\left(l_{2i'} \frac{\partial^2 w}{\partial x_i' \partial x_j'} l_{2j'} + \mu l_{1i'} \frac{\partial^2 w}{\partial x_i' \partial x_j'} l_{1j'} \right) \tag{11}$$

$$\sigma_{12} = -\frac{Ez}{1+\mu} \left[1 + 0.208 l^2 \left(\frac{\partial^2}{\partial x_1'^2} + \frac{\partial^2}{\partial x_2'^2} \right) \right] l_{1i'} \frac{\partial^2 w}{\partial x_i' \partial x_j'} l_{2j'}$$

In the global coordinate (x_1', x_2'), the stress components are

$$\sigma_{ij}' = \sigma_{i'j'} = l_{i'j} \sigma_{ij} l_{ij'} \tag{12}$$

2.4 Physic equations

The normal and shear stresses can be collected into bending moment M_{11}', M_{22}' and torque M_{12}', respectively.

$$\left. \begin{array}{l} M_{11}' = -\displaystyle\int_{-\frac{h}{2}}^{\frac{h}{2}} \sigma_{11}' z \, dz \\[3mm] M_{22}' = -\displaystyle\int_{-\frac{h}{2}}^{\frac{h}{2}} \sigma_{22}' z \, dz \\[3mm] M_{12}' = -\displaystyle\int_{-\frac{h}{2}}^{\frac{h}{2}} \sigma_{12}' z \, dz \end{array} \right\} \tag{13}$$

The bending equilibrium equation of the plate on which a distribution force q is applied

$$\frac{\partial^2 M_{11}'}{\partial x_1'^2} + 2 \frac{\partial^2 M_{12}'}{\partial x_1' \partial x_2'} + \frac{\partial^2 M_{22}'}{\partial x_2'^2} + q = 0 \tag{14}$$

Combination of Eqs. (11)–(14) yields

$$A_1 \left(\frac{\partial^6 w}{\partial x_2'^6} + \frac{\partial^6 w}{\partial x_1'^6} \right) + A_2 \left(\frac{\partial^6 w}{\partial x_1' \partial x_2'^5} - \frac{\partial^6 w}{\partial x_1'^5 \partial x_2'} \right) + A_3 \left(\frac{\partial^6 w}{\partial x_1'^2 \partial x_2'^4} + \frac{\partial^6 w}{\partial x_1'^4 \partial x_2'^2} \right)$$

$$+ A_4 \left(\frac{\partial^4 w}{\partial x_2'^4} + \frac{\partial^4 w}{\partial x_1'^4} \right) + A_5 \frac{\partial^4 w}{\partial x_1'^2 \partial x_2'^2} = \frac{q}{D} \tag{15}$$

Where $D = \dfrac{Eh^3}{12(1-\mu^2)}$

$$\begin{cases} A_1 = 0.208 l \left(\sin^6 \beta + \cos^6 \beta \right) - 0.362 l \cos^2 \beta \sin^2 \beta \\ A_2 = 0.30784 l \cos \beta \sin^3 \beta - 0.30784 l \cos^3 \beta \sin \beta \\ A_3 = 0.05408 l \left(\sin^6 \beta + \cos^6 \beta \right) + 0.416 l \left(1 - 3.76 \cos^2 \beta \sin^2 \beta \right) \\ A_4 = \sin^4 \beta - 1.48 \sin^2 \beta \cos^2 \beta + \cos^4 \beta \\ A_5 = 2.52 \sin^4 \beta - 1.92 \sin^2 \beta \cos^2 \beta + 2.52 \cos^4 \beta \end{cases} \tag{16}$$

3   Numerical examples and discussions

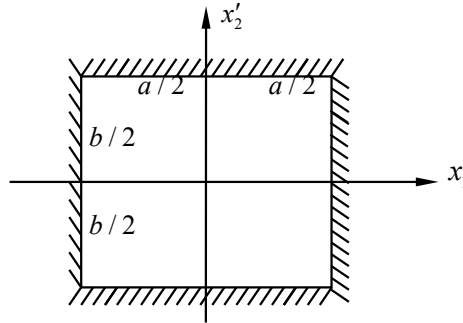A clamped rectangle graphene sheet is shown as Fig. 3.

Figure 3: A clamped rectangle graphene sheet.

The boundary conditions of the clamped graphene sheet can be written as

$$
\begin{cases}
w|_{x_1'=-a/2,a/2}=0,\ \dfrac{\partial w}{\partial x_1'}|_{x_1'=-a/2,a/2}=0 \\[2mm]
w|_{x_2'=-b/2,b/2}=0,\ \dfrac{\partial w}{\partial x_2'}|_{x_2'=-b/2,b/2}=0
\end{cases}
\tag{17}
$$

Where a and b are, respectively, the length and the width of the graphene sheet.

The deflection expression of the graphene sheet in terms of Galerkin method is given by

$$
w=\sum_m C_m w_m = \left(x_1'^2-\frac{a^2}{4}\right)^2\left(x_2'^2-\frac{b^2}{4}\right)^2\left(C_1+C_2x_1'^2+C_3x_2'^2+\ldots\right)
\tag{18}
$$

Eq. (18) are consistent with the clamped boundary conditions of the graphene sheet.

Galerkin weak form of Eq. (15) is given by

$$
\begin{aligned}
\int_{-a}^{a}\int_{-b}^{b}&\left[A_1\left(\frac{\partial^6 w}{\partial x_2'^6}+\frac{\partial^6 w}{\partial x_1'^{56}}\right)+A_2\left(\frac{\partial^6 w}{\partial x_1'\partial x_2'^5}-\frac{\partial^6 w}{\partial x_1'^5\partial x_2'}\right)\right. \\[2mm]
&+A_3\left(\frac{\partial^6 w}{\partial x_1'^2\partial x_2'^4}+\frac{\partial^6 w}{\partial x_1'^4\partial x_2'^2}\right)+A_4\left(\frac{\partial^4 w}{\partial x_2'^4}+\frac{\partial^4 w}{\partial x_1'^4}\right) \\[2mm]
&\left.+A_5\frac{\partial^4 w}{\partial x_1'^2\partial x_2'^2}\right]w_m\mathrm{d}x_1'\mathrm{d}x_2'=\int_{-a}^{a}\int_{-b}^{b}\frac{q}{D}w_m\mathrm{d}x_1'\mathrm{d}x_2'
\end{aligned}
\tag{19}
$$

Where $m=1,2,3,\ldots$

The approximate solution of Eq. (19) is given as following

$$w = \sum_{m=1}^{3} C_m w_m = \left(x_1'^2 - \frac{a^2}{4}\right)^2 \left(x_2'^2 - \frac{b^2}{4}\right)^2 \left(C_1 + C_2 x_1'^2 + C_3 x_2'^2\right) \tag{20}$$

Where

$$w_1 = \left(x_1'^2 - \frac{a^2}{4}\right)^2 \left(x_2'^2 - \frac{b^2}{4}\right)^2 \tag{21}$$

$$w_2 = \left(x_1'^2 - \frac{a^2}{4}\right)^2 \left(x_2'^2 - \frac{b^2}{4}\right)^2 x_1'^2 \tag{22}$$

$$w_3 = \left(x_1'^2 - \frac{a^2}{4}\right)^2 \left(x_2'^2 - \frac{b^2}{4}\right)^2 x_2'^2 \tag{23}$$

Substituting of Eqs. (21)–(23) into Eq. (19) has

$$
\begin{cases}
\int_{-a}^{a} \int_{-b}^{b} \left[A_1 \left(\frac{\partial^6 w}{\partial x_2'^6} + \frac{\partial^6 w}{\partial x_1'^{56}} \right) + A_2 \left(\frac{\partial^6 w}{\partial x_1' \partial x_2'^5} - \frac{\partial^6 w}{\partial x_1'^{55} \partial x_2'} \right) \right. \\
\qquad + A_3 \left(\frac{\partial^6 w}{\partial x_1'^2 \partial x_2'^4} + \frac{\partial^6 w}{\partial x_1'^4 \partial x_2'^2} \right) + A_4 \left(\frac{\partial^4 w}{\partial x_2'^4} + \frac{\partial^4 w}{\partial x_1'^4} \right) \\
\qquad \left. + A_5 \frac{\partial^4 w}{\partial x_1'^2 \partial x_2'^2} \right] \left(x_1'^2 - \frac{a^2}{4} \right)^2 \left(x_2'^2 - \frac{b^2}{4} \right)^2 \mathrm{d}x_1' \mathrm{d}x_2' \\
= \int_{-a}^{a} \int_{-b}^{b} \frac{q}{D} \left(x_1'^2 - \frac{a^2}{4} \right)^2 \left(x_2'^2 - \frac{b^2}{4} \right)^2 \mathrm{d}x_1' \mathrm{d}x_2' \\[6pt]
\int_{-a}^{a} \int_{-b}^{b} \left[A_1 \left(\frac{\partial^6 w}{\partial x_2'^6} + \frac{\partial^6 w}{\partial x_1'^{56}} \right) + A_2 \left(\frac{\partial^6 w}{\partial x_1' \partial x_2'^5} - \frac{\partial^6 w}{\partial x_1'^{55} \partial x_2'} \right) \right. \\
\qquad + A_3 \left(\frac{\partial^6 w}{\partial x_1'^2 \partial x_2'^4} + \frac{\partial^6 w}{\partial x_1'^4 \partial x_2'^2} \right) + A_4 \left(\frac{\partial^4 w}{\partial x_2'^4} + \frac{\partial^4 w}{\partial x_1'^4} \right) \\
\qquad \left. + A_5 \frac{\partial^4 w}{\partial x_1'^2 \partial x_2'^2} \right] \left(x_1'^2 - \frac{a^2}{4} \right)^2 \left(x_2'^2 - \frac{b^2}{4} \right)^2 x_1'^{52} \mathrm{d}x_1' \mathrm{d}x_2' \\
= \int_{-a}^{a} \int_{-b}^{b} \frac{q}{D} \left(x_1'^2 - \frac{a^2}{4} \right)^2 \left(x_2'^2 - \frac{b^2}{4} \right)^2 x_1'^2 \mathrm{d}x_1' \mathrm{d}x_2' \\[6pt]
\int_{-a}^{a} \int_{-b}^{b} \left[A_1 \left(\frac{\partial^6 w}{\partial x_2'^6} + \frac{\partial^6 w}{\partial x_1'^{56}} \right) + A_2 \left(\frac{\partial^6 w}{\partial x_1' \partial x_2'^5} - \frac{\partial^6 w}{\partial x_1'^{55} \partial x_2'} \right) \right. \\
\qquad + A_3 \left(\frac{\partial^6 w}{\partial x_1'^2 \partial x_2'^4} + \frac{\partial^6 w}{\partial x_1'^4 \partial x_2'^2} \right) + A_4 \left(\frac{\partial^4 w}{\partial x_2'^4} + \frac{\partial^4 w}{\partial x_1'^4} \right) \\
\qquad \left. + A_5 \frac{\partial^4 w}{\partial x_1'^2 \partial x_2'^2} \right] \left(x_1'^2 - \frac{a^2}{4} \right)^2 \left(x_2'^2 - \frac{b^2}{4} \right)^2 x_2'^{52} \mathrm{d}x_1' \mathrm{d}x_2' \\
= \int_{-a}^{a} \int_{-b}^{b} \frac{q}{D} \left(x_1'^2 - \frac{a^2}{4} \right)^2 \left(x_2'^2 - \frac{b^2}{4} \right)^2 x_2'^2 \mathrm{d}x_1' \mathrm{d}x_2'
\end{cases} \tag{24}
$$

C_1, C_2 and C_3 can be obtained from the solution of Eq. (24).

Classical static deflection of the graphene sheet can be obtained by substituting $l = 0$ into Eq. (19).

To illustrate the small-scale effect on the static deflections of the graphene sheet , the small- scale effect factor η is defined as

$$\eta = \frac{w_{cs}}{w_{ns}} \tag{25}$$

Where w_{cs} and w_{ns} are, respectively, the classical and nonlocal static deflections of the center point of the graphene sheet

For all the subsequent numerical example, the length of C-C bond $l = 0.142 \times 10^{-9}$ m, in-plane stiffness $Eh = 360$ J/m^2 (Sanchez-Portal, D, 1999), Poisson's ratio $\mu = 0.26$, the thickness of the graphene sheet $h = 0.34$ nm.

To investigate the effect of the small-scale on the static deflection of the graphene sheet, we calculated the small-scale effect factor η of the graphene sheets with the different helical angles and geometric sizes.
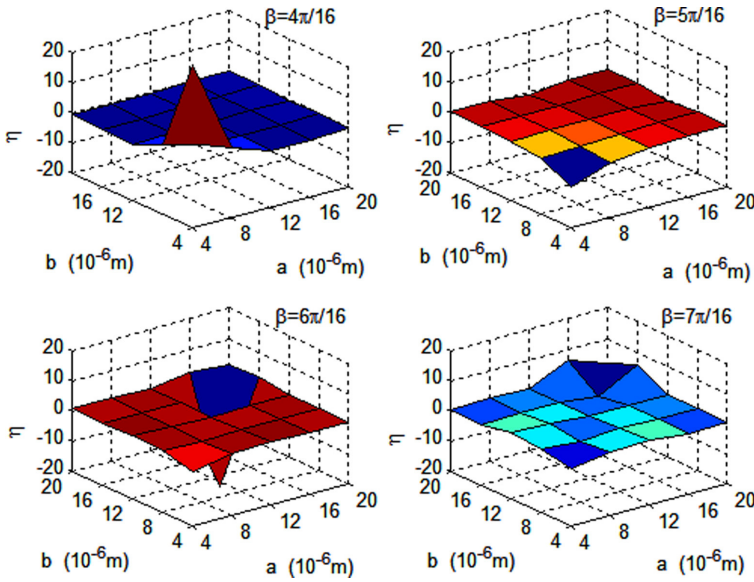

Figure 4: Small-scale effect factor of the static deflection of the center point of the graphene sheet with the different helical angles and geometric sizes (4 um $\leq a \leq$ 20 um, 4 um $\leq b \leq$ 20 um).

Fig. 4 shows that small-scale effect factor of the static deflection of the center point of the graphene sheet with the different helical angles and geometric sizes

(4 um $\leq a \leq$ 20 um, 4 um $\leq b \leq$ 20 um). It can be found From Fig. 4 that the small-scale effect factor η is influence by the helical angle of the graphene sheet. The small-scale effect factor is far from 1, the small-scale effect is very obvious when the side length of the helical graphene sheet is smaller than 20 um. the small-scale effect will not always decrease with increase of the geometrical size of the helical graphene sheet.

Fig. 5 shows that small-scale effect factor of the static deflection of the center point of the graphene sheet with different helical angles and geometric sizes (4 um $\leq a \leq$ 20 um, 4 um $\leq b \leq$ 20 um). It can be seen from comparison of Fig. 5 and Fig. 4 that the small-scale effect factor η changes periodically with change of helical angle, the change cycle is $\pi/4$.
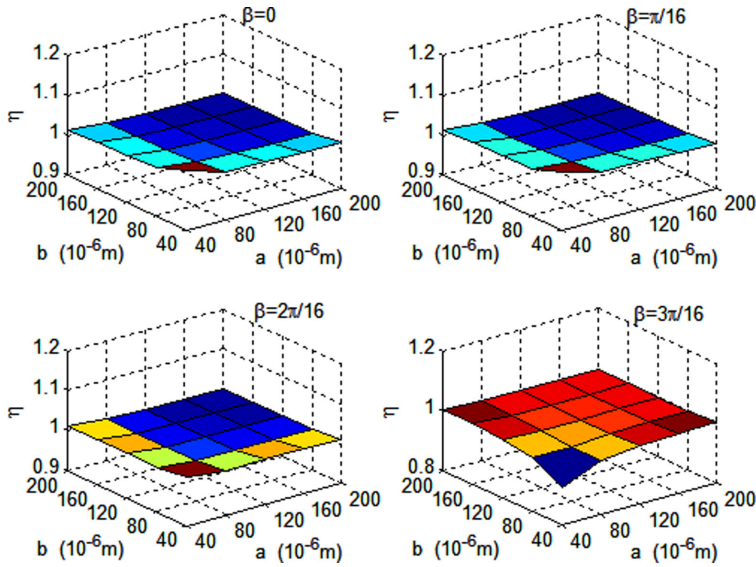

Figure 5: Small-scale effect factor of the static deflection of the center point of graphene sheet with the different helical angles and geometric sizes (4 um $\leq a \leq$ 20 um, 4 um $\leq b \leq$ 20 um).

Fig. 6 shows that small-scale effect factor of the static deflection of the center point of the graphene sheet with the different helical angles and geometric sizes (40 um $\leq a \leq$ 200 um, 40 um $\leq b \leq$ 200 um). It can be seen from Fig. 6 that the small-scale effect factor η is more and more close to 1 with increase of the side length of the graphene sheet no matter how much the helix angle is. When the length and the width of the helical graphene sheet are both larger than 200um, the small-scale effect of the static deflection of the graphene sheet almost disappears.
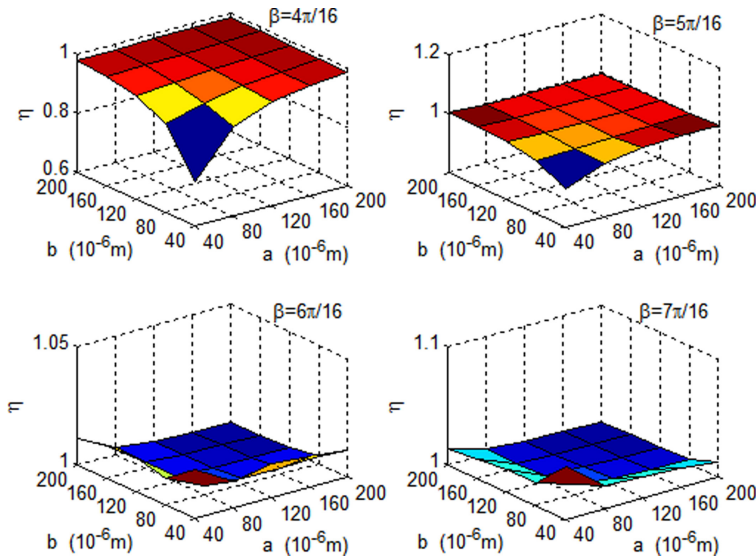
Figure 6: Small-scale effect factor of the static deflection of the center point of the graphene sheet with the different helical angles and geometric dimensions (40 um ≤ a ≤ 200 um, 40 um ≤ b ≤ 200 um).

Figure 7: small-scale effect factor of the static deflection of the center point of the graphene sheet with the different helical angles and geometric sizes (40 um ≤ a ≤ 200 um, 40 um ≤ b ≤ 200 um).

Fig. 7 shows that small-scale effect factor of the static deflection of the center point of the graphene sheet with the different helical angle and geometric sizes (40 um $\leq a \leq$ 200 um, 40 um $\leq b \leq$ 200 um).It can be seen from comparison of Fig. 6 and Fig. 7 that the small-scale effect factor η will change periodically with change of helical angle, the change cycle is $\pi/4$.

Fig. 8 shows that comparison of small-scale effect factor of the static deflection of the graphene sheet with the different helical angles (40 um $\leq a \leq$ 200 um, 40 um $\leq b \leq$ 200 um). It can also be found from Fig. 8 that the small-scale effect factor η of the same geometrical dimension graphene sheet will increase when the helical angles change from $\beta = 0$ to $\beta = 4\pi/16$. In other words, the small-scale effect of the same geometrical dimension graphene sheet will decrease with increase of its helical angle from $\beta = 0$ to $\beta = 4\pi/16$.
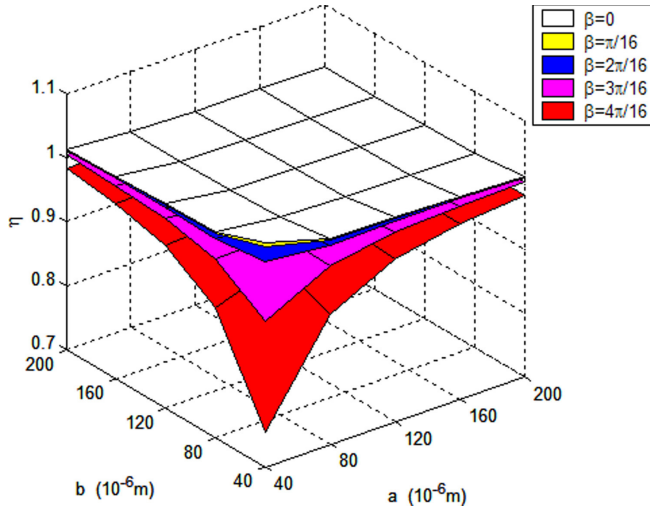

Figure 8: Comparison of small-scale effect factor of the static deflection of the graphene sheet with the different helical angles.

Fig. 9 shows that comparison of small-scale effect factor of the static deflection of the graphene sheet with the different helical angles. It can also be found from Fig. 9 that the small-scale effect factor η of the same geometrical dimension graphene sheet will increase when the helical angles change from $\beta = \dfrac{4\pi}{16}$ to $\beta = 8\pi/16$. Combination of Fig. 8 with Fig. 9, it can be seen that the small-scale effect factor η of the same geometrical dimension helical graphene sheet has a periodic change of $\beta = \pi/4$ with the change of the helical angle.

Fig. 10 shows that comparison of the static deflection of the center point of the
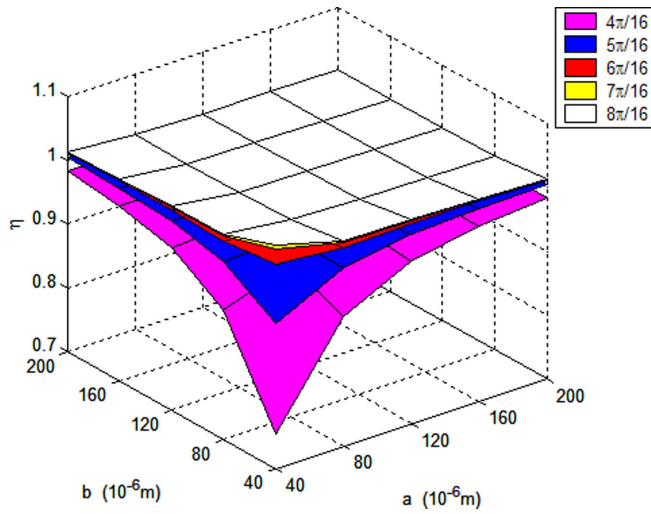
Figure 9: Comparison of small-scale effect factor of the static deflection of the graphene sheet with the different helical angles.
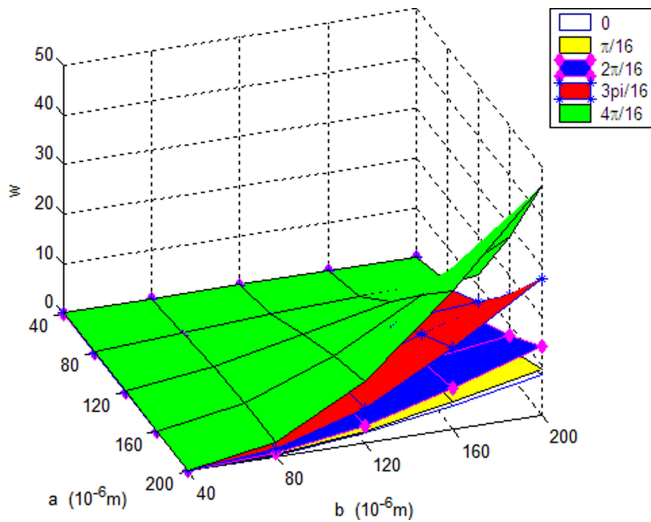

Figure 10: Comparison of the static deflection of the center point of the graphene sheet with the different helical angles and geometrical dimensions.

graphene sheet with the different helical angles. It can be seen from Fig. 10 that the static deflection of the center point of the graphene sheet will increase when the helical angle of the same length and width graphene sheet increases from $\beta = 0$
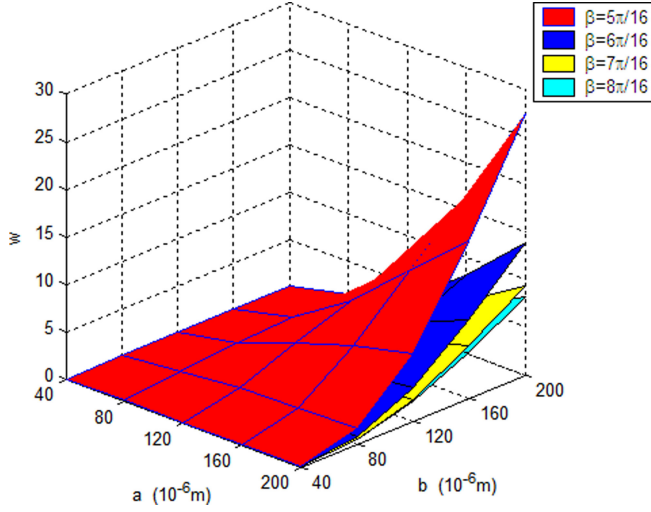
Figure 11: Comparison of the static deflections of the center point of the graphene sheet with the different helical angles and geometrical dimensions.

to $\beta = 4\pi/16$ or the length and width of the same helical angle graphene sheet increases.

Fig. 11 shows that comparison of the static deflection of the center point of the graphene sheet with the different helical angles. It can be seen from Fig. 11 that the static deflection of the center point of the graphene sheet will increase when the helical angle of the same length and width graphene sheet decreases from $\beta = 8\pi/16$ to $\beta = 4\pi/16$ or when the length and width of the same helical angle graphene sheet increases. The static deflection of the same geometrical dimension helical graphene sheet has a periodic change of $\beta = \pi/4$ with the change of the helical angle.

4   Conclusion

Taking the typical hexagonal element of the graphene sheet as the research object, based on the concept of nonlocal theory, the stress tensor of any point within the typical element is expanded into Taylor series, the nonlocal constitutive equations of the graphene sheet was established. Galerkin weak form is used to solve the equilibrium equation of the graphene sheet. The classical and the nonlocal static deflections of the graphene sheet were obtained from solution of the equilibrium equation. To illustrate the small-scale effect on the static deflections of the graphene sheet, the small-scale effect factor is defined as the ratio of the static deflections of

the center point of the classical plate to that of the nonlocal plate.

Numerical results show that

1. When the length and width of the graphene sheet are less than 20 um, the small-scale effect factor of the static deflection of the graphene sheet will be very large, the small-scale effect is very obvious, and the small-scale effect will not always decrease with increase of the geometrical dimensions of the helical graphene sheet, the small-scale effect factor η is influence by the helical angle of the graphene sheet

2. For 40 um $\leq a \leq$ 200 um, 40 um $\leq b \leq$ 200 um, small-scale effect factor of the static deflection of the graphene sheet is more and more close to 1 with the increase of the length and width of the graphene sheet, the small-scale effect will disappear when the length and the width of the plate are both larger than 200um.When the helical angle of the graphene sheet changes from 0 to $\pi/4$, The small-scale effect will decrease.

3. For the same geometrical dimension graphene sheet, the small-scale effect factor has a periodic change of $\beta = \pi/4$ with the change of the helical angle.

4. The static deflection of the center point of the graphene sheet will increase when the helical angle of the same length and width graphene sheet reduces from $\beta = 0$ to $\beta = 4\pi/16$ or when the length and width of the same helical angle graphene sheet increases. The static deflection has a periodic change of $\beta = \pi/4$ with the change of the helical angle.

References

Eringen, A. C. (1983): On differential equations of nonlocal elasticity and solutions of screw dislocation and surface waves. *Journal of Applied Physics*. vol. 54, no. 9, pp. 4703–4710.

Eringen, A. C.; Edelen, D. G. B. (1972): On nonlocal elasticity. *Int. J. Enging*, no. 10, pp. 233–248.

Fang, B.; Zhen, Y. X.; Zhang, C. P. (2013): Nonlinear vibration analysis of double-walled carbon nanotubes based on nonlocal elasticity theory. *Appl. Math. Modeling*, vol. 37, no. 3, pp. 1096–1107.

Iijima, S. (1991): Helical microtubes of graphitic carbon. *Nature*. vol. 354, pp. 56–58.

Liang, Y.; Han, Q. (2014): Prediction of the nonlocal scaling parameter for graphene sheet. *European Journal of Mechanics-A/Solids*, vol. 45, pp. 153–160.

Miandoab, E. M.; Yousefi-Koma, A.; Pishkenari, H .N. (2015): Nonlocal and strain gradient based model for electrostatically actuated silicon nano-beams. *Microsystem Technologies*, vol. 21, no. 2, pp. 457–464.

Reddy, J. N. (2010): Nonlocal nonlinear formulations for bending of classicalal and shear deformation theories of beams and plates. *Int. J. Eng. Sci.*, vol. 48, no. 11, pp. 1507–1518.

Sanchez-Portal, D.; Emilio A. (1999): A study based on ab initio structural, elastic, and vibrational properties of carbon nanotubes, *Phys. Rev. B*, vol. 59, no. 18, pp. 12678–12688.

Wang, L. (2011): A modified nonlocal beam model for vibration and stability of nanotubes conveying fluid. *Phys. E.*, vol. 44, no. 1, pp. 25–28.

Xie, G. Q.; Han, X.; Long, S. Y. (2006): Effect of small-scale scale on the radial Buckling pressure of a clamped multi-walled carbon nanotube. *Smart Mater. and Struct.*, vol. 15, no. 4, pp. 1143–1149.

Xie, G. Q.; Han, X.; Long, S. Y. (2007): Long. The effect of the small-scale on dispersion characteristics of the carbon nanotube. *Int. J. Solid. Struct.*, vol. 44, no. 4, pp. 1242–1255.

Xie, G. Q.; Long, S. Y. (2006): Elastic vibration behaviors of carbon nanotubes based on micropolar mechanics. *CMC: Computers, Materials & Continua*, vol. 4, no. 2, pp. 11–20.

Zhang, Y. Q.; Liu, G. R.; Wang, J. S. (2004): Small scale effects on buckling of multi-walled carbon nanotubes under axial compression. *Phys. rev. B*, vol. 70, no. 20, pp. 205430.

Zhang, Y. Y.; Wang, C. M.; Challamel, N. (2009): Bending, buckling, and vibration of micro/nanobeams by hybrid nonlocal beam model. *J. eng. Mech.*, vol. 136, no. 5, pp. 562–574.

Zhao, P.; Shi, G. (2011): Study of Poisson Ratios of Single-Walled Carbon Nanotubes based on an Improved Molecular Structural Mechanics Model. *CMC: Computers, Materials & Continua*, vol. 22, no. 2, pp. 147–168.